Abstract

The diagnostics of large scale geostrophy in a stratified atmosphere are revisited using a full Coriolis force. This formulation of geostrophy includes the horizontal and vertical projections of the planetary rotation vector, accounts for the spherical geometry of the atmosphere, is not singular at the equator, and provides partial information about vertical transport. The accuracy of the standard hydrostatic approximation in the geostrophic regime is gauged and an alternative is discussed. The standard hydrostatic approximation predicts much smaller wind shears than those derived from the primitive equations. The observations are a set of global temperature maps of the upper Jovian troposphere at four pressure levels, between 100 and 400 mbar, obtained from mid-infrared observations in June, 1996. Maps of the large-scale thermal shears show higher concentration of longitudinal structures and vertical transport along two particular zonal bands at latitudes near 15°N and 15°S. Observational criteria are proposed to validate the standard versus the new diagnostic as well as the possible geostrophic regime of Jupiter's zonal jets.

1 Introduction

Explaining the ability of planetary flows to display very robust large scale organization remains a challenging problem in planetary sciences. The structure of the Jovian zonal winds is one example of such organization. Several models have attempted to identify the agent driving these jets in Jupiter (*Rhines,* 1975; *Williams & Robinson,* 1973; *Busse,* 1976; *Cho & Polvani,* 1996; *Williams,* 1996). Each model assumes that, on the large scale, Jupiter is dominated by one of several possible dynamical regimes. The separate claim is that the mechanism is understood, but each explanation is providing different answers and can explain only different aspects of the large scale jet structure. Geostrophic dynamics (*Rhines,* 1975) is considered one of the most likely regimes. Geostrophy is defined as the dynamical balance between the Coriolis forces and the horizontal pressure gradients in an atmosphere. Such conditions are found in very rapidly rotating planets like Jupiter. In geostrophic balance, diabatic effects can generate horizontal entropy gradients that separate the different thermodynamic variables from their hydrostatic profile, thus causing geostrophic winds. The geostrophic model of the large scale banded structure of Jupiter is based on the assumption that diabatic effects are not strong enough to significantly distort the wind pattern caused by the geostrophic regime. In this regime, the latitudinal variation of the Coriolis force, the β effect, introduces one length scale, the *Rhines scale*, that coincides with the scale of the Jovian jets, but the discontinuity of geostrophic balance at the equator raises doubts on the application of this model at planetary scale. It has been argued that this discontinuity is an arctifact of the partial representation of the Coriolis force in the primitive equation approach (*Veronis,* 1968; *de Verdière & Schopp,* 1994) on which geostrophic models and diagnostics are based. It is thus relevant to address the effects of a full Coriolis force. A full representation of the Coriolis force lacks the traditional singularity of geostrophy at the equator extending the possibility of geostrophic balance at all latitudes (*Veronis,* 1968; *de Verdière & Schopp,* 1994). This advantage will be

gradients along isobars can be inferred from the temperature gradients measured by IR maps. The temperature fields so derived can be used as a surrogate for horizontal density gradients under the geostrophic approximation. Since Jupiter's high rotation rate makes geostrophic balance very plausible, thermal IR observations offer a useful tool to infer the wind circulation in the upper troposphere and lower stratosphere. Voyager IR measurements covering irregular, but dense, grids of Jupiter have been used previously to create zonally averaged temperature profiles from which mean winds were inferred using the primitive equation approach (*e.g.* (*Pirraglia et al.,* 1981; *Gierasch,* 1986)). The zonal geostrophic winds derived by these authors seemed consistent with cloud tracking results under the geostrophic balance assumption. A recent review, (*Gierasch,* 1993), pointed out, however, the absence of global maps with regular coverage of the full planet. Unlike previous IR data sets, ground based observations provide latitude-longitude maps with constant longitudinal resolution and high signal-to-noise ratio above the clouds.

Section 2 of this work reviews the differences between the full and the primitive equations. Section 3 reviews geostrophy in the primitive equation approach to help the comparison with section 4 where the the full 3-d version of geostrophic balance, its effect on the hydrostatic approximation and the thermal wind diagnostics are discussed. Section 5 discusses the error involved in neglecting the nonhydrostatic and the nonlinear terms. In section 6 the observations methods are described. Finally, section 7 discusses the results in light of the previous sections before presenting the conclusions in section 8.

2 The full and the primitive equations

Atmospheric dynamics are described by the equations of gas flow in a spherical shell geometry:

These equations are understood as a Reynolds-like spatial average in which all viscosities have been neglected. For our work, the averaging scale is set by the resolution of observations in a similar way as numerical grids set the resolution scale of computational models. This system of coupled nonlinear equations is too complex for direct application in diagnostics since accurate use requires fully nonlinear, 3-dimensional codes in a spherical geometry. Significant progress is usually achieved by making assumptions which result in simplifications of the equations. The frequent approach is to substitute the full equations by the primitive equations. Then, two assumptions, geostrophic and hydrostatic balance, are applied. Geostrophic and hydrostatic balance are crucial for diagnostic methods based on IR-data.

The primitive equations set the foundations for atmospheric dynamics and for the traditional formulation of geostrophy. They are justified from scale analysis of the continuity equation in atmospheric layers where the depth scale is comparable to the density scale *e.g.* (*Gill,* 1982; *Houghton,* 1986; *Pedlosky,* 1987; *Holton,* 1992). Shallowness of atmospheric layers suggests much smaller vertical than horizontal velocities. Therefore, the vertical velocities and accelerations are neglected in the momentum equations. The neglected terms also involve the horizontal projection of the planetary rotation vector. As a consequence, only the vertical component of the rotation vector, $f \equiv 2\Omega \sin\lambda$, is considered. The insufficiency of this approach has been subject of a long standing debate (*Veronis,* 1968; *Phillips,* 1968). Other extra assumptions used in this context involve using the *small gap approximation* (the radial variable is assumed constant in the derivatives) and neglecting the curvature terms wv/r, v^2/r (for a discussion see (*White & Bromley,* 1995)).

Geostrophic balance is defined as the balance between the Coriolis forces and the other forces, that is:

$$2\Omega\vec{k} \wedge \vec{v}_g = -\frac{1}{\rho}\vec{\nabla}\pi + \vec{g} + O(Ro) \tag{1}$$

The predictions of the two descriptions of geostrophic balance differ completely. The most significant being that the full formulation does not diverge at equatorial latitudes. Dropping the horizontal component of the planetary rotation is responsible for the singularity in the traditional geostrophic approximation at the equator because the physics near the equator are ill-represented. Close to the equator, Taylor-Proudman columns aligning parallel to the full rotation vector would become perpendicular to the local horizontal, but this result is prevented in the primitive equations. Another difference affects the hydrostatic approximation which is inconsistent with geostrophy with a full Coriolis force (*de Verdière & Schopp,* 1994).

3 Geostrophic winds in the primitive equations

It is customary to separate pressure into its hydrostatic and non-hydrostatic contributions by introducing a perturbation parameter ϵ such that: $\pi = p_h(z) + \epsilon\pi_1(x,y,z)$. The basic state is given by the solution to *hydrostatic balance*: $\vec{\nabla}p_h = \rho\vec{g}$. Hydrostatic balance is a barotropic solution to the momentum equations with $\vec{v} = \vec{0}$. In hydrostatic equilibrium, where gravity is in the vertical direction, pressure and, therefore, density depend only on z. The equation of state $p(\rho, T)$ then implies that, temperature depends only on z in hydrostatic balance. This justifies the expansions $T = T_h(z) + \epsilon_T T_1(x,y,z) + O(\epsilon_T^2)$, where T_h is defined as the basic temperature profile at which hydrostatic balance (no buoyancy) holds, and $\rho(p,T) = \rho_h\left[1 - \alpha_T(T - T_h) + \kappa(p - p_h) + O(\epsilon_\rho^2)\right]$ where, $\alpha_T = -\frac{1}{\rho_h}\left(\frac{\partial\rho}{\partial T_h}\right)_p$ is the coefficient of thermal expansion, and $\kappa = \frac{1}{\rho_h}\left(\frac{\partial\rho}{\partial p_h}\right)_T$ is the coefficient of isothermal compressibility. $\pi_1/p_h \sim 1$. This expansion is needed for non-ideal gases or out of equilibrium thermodynamics. In an ideal gas in equilibrium $\alpha_T = 1/T_h$, $\kappa = 1/p_h$. We allow for different perturbation parameters $\epsilon_T \neq \epsilon \neq \epsilon_\rho$ to account for situations where temperature, pressure, and density deviations have different magnitudes. It will be shown later that $\epsilon_\rho \ll \epsilon$ and thus, $\epsilon_T \sim \epsilon$. Jupiter's atmosphere is in a diabatic situation out of equilibrium where uniform internal heating largely dominates

perturbation is refered to as the "standard" or the "classical" hydrostatic approximation. The hydrostatic approximation only means that the vertical pressure profile is not determined by hydrostatic balance, but horizontal pressure gradients are possible.

Pressure is difficult to measure by remote sensing, and thus an alternative widely used in IR diagnostics are the thermal wind equations (*e.g.* (*Gierasch,* 1986; *Magalhães et al.,* 1990; *Orton,* 1994)). This alternative returns the vertical gradients of the geostrophic winds so that, if they are known at a pressure level, the winds can be derived through integration. This alternative has the advantage of requiring only knowledge of the temperature field. Instead of using the pressure gradient term $\frac{1}{\rho}\vec{\nabla}\pi$, it is standard practice to define the geopotential as $\Phi(x,y,z) = -\int_{z_o}^{z} g dz$, such that, from the hydrostatic approximation, $\frac{\partial\Phi}{\partial p} = -\frac{1}{\rho} = -\frac{RT}{M_r p}$. In terms of Φ, the geostrophic velocities (3) are, $u_g = -\frac{1}{f}\frac{\partial\Phi}{\partial y}$ and $v_g = \frac{1}{f}\frac{\partial\Phi}{\partial x}$. Following *e.g.* (*Holton,* 1992) pp. 74-75, if these identities are differentiated with respect to pressure and the differential is multiplied by pressure yields:

$$\frac{\partial u_g}{\partial z^*} = -p\frac{\partial u_g}{\partial p} = p\frac{\partial}{\partial p}\left(\frac{1}{f}\frac{\partial\Phi}{\partial y}\right)_p = p\frac{1}{f}\frac{\partial}{\partial y}\left(\frac{\partial\Phi}{\partial p}\right) = -p\frac{1}{f}\frac{\partial}{\partial y}\left(\frac{1}{\rho}\right)_p = -\frac{R}{fM_r}\left(\frac{\partial T}{\partial y}\right)_p$$

and

$$\frac{\partial v_g}{\partial z^*} = -p\frac{\partial v_g}{\partial p} = -p\frac{\partial}{\partial p}\left(\frac{1}{f}\frac{\partial\Phi}{\partial x}\right)_p = -p\frac{1}{f}\frac{\partial}{\partial x}\left(\frac{\partial\Phi}{\partial p}\right) = p\frac{1}{f}\frac{\partial}{\partial x}\left(\frac{1}{\rho}\right)_p = \frac{R}{fM_r}\left(\frac{\partial T}{\partial x}\right)_p$$

where $z = Hz^* = -Hln(p_h/p_0)$, with $H = RT_h/g$ being the pressure scale-height.

What leads to the traditional thermal wind relations:

$$\begin{cases} \frac{\partial u_g}{\partial z^*} &= -\frac{R}{fM_r}\left(\frac{\partial T}{\partial y}\right)_p + O(w, \epsilon Ro, \epsilon^2) \\ \frac{\partial v_g}{\partial z^*} &= \frac{R}{fM_r}\left(\frac{\partial T}{\partial x}\right)_p + O(w, \epsilon Ro, \epsilon^2). \end{cases} \tag{4}$$

For the later comparison, it is worth to note here that in its customary application in diagnostics, x and y are the horizontal variables. This involves assuming that the permutations of the derivatives for the derivation of (4) remain valid, which holds if that $\partial p/\partial x = \partial p/\partial y = 0$. This identity is truth if pressure is understood as the hydrostatic profile and one neglects the horizontal contributions contained in $\epsilon\pi_1$.

a different approach. It can be seen easily that if the small gap approximation used in shallow layers is used to calculate the divergence, the continuity equation leads to the condition: $g\frac{\epsilon_\rho}{\epsilon}\frac{\partial \rho_1}{\partial x}\cos\lambda = \frac{1}{r}\frac{\partial \pi_1}{\partial x}$, which does not diverge either. Both conditions suggest that, except at the poles, the ratio of the density perturbations to the pressure perturbations is $\epsilon_\rho/\epsilon \sim 1/(gr) \ll 1$.

It has been noted for the unstratified case (*de Verdière & Schopp,* 1994) that geostrophic balance with a full Coriolis force is incompatible with the hydrostatic approximation. This happens because (5) can have a solution only if its right hand side is perpendicular to the rotation vector $\vec{k}$. This is, if: $\vec{k}\cdot(\vec{\nabla}\pi - \rho\vec{g}) = \epsilon\vec{k}\cdot(\vec{\nabla}\pi_1 - \frac{\epsilon_\rho}{\epsilon}\rho_1\vec{g}) + O(\epsilon^2) = O(\epsilon^2)$. In a manner that will prove useful later, this condition reads:

$$\frac{1}{\rho}\frac{\partial \pi_1}{\partial Z} + \frac{\epsilon_\rho}{\epsilon}\frac{\rho_1}{\rho}g\sin\lambda = \frac{\cos\lambda}{\rho}\frac{\partial \pi_1}{\partial y} + \frac{\sin\lambda}{\rho}\left(\frac{\partial \pi_1}{\partial z} + \frac{\epsilon_\rho}{\epsilon}\rho_1 g\right) = O(\epsilon) \tag{7}$$

This condition can be seen as reflecting that the zonal velocities involved in the meridional and vertical momentum equations have to be consistent with each other. One can see (7) as the planetary scale version of the "hydrostatic approximation" since this identity reduces to the hydrostatic approximation under the assumption that only the vertical rotation is important. If the nonlinear contribution for low Rossby numbers is being included in π_1, this condition remains valid in the nonlinear regime to order ϵ^1. If this relation is used in (6), the zonal velocity becomes: $u_g = -\frac{1}{2\Omega\rho\sin\lambda}\frac{\partial \pi_1}{\partial y} + O(\epsilon)$. This result coincides with the traditional expression derived from the primitive equations, which is suprising since there are significant differences in the number of terms used and in the fact that the hydrostatic approximation is not used in this section. The meridional and vertical components remain, however, different from the standard prediction.

The standard hydrostatic approximation is a deeply entrenched assumption, applied even in formulations with a full Coriolis force (*White & Bromley,* 1995). It may be illustrative to adress also the results obtained with a full geostrophy and the hydrostatic approximation for the sake of comparison. In that case, the velocity is not a solution to

equation is the curl of the momentum equation. After multiplying by density, the curl of (5) leads to:

$$-\epsilon(2\vec{\Omega}\cdot\vec{\nabla})(\rho\vec{v_g}) = \vec{\nabla}\rho\wedge\vec{g}. \tag{8}$$

This expression includes the full planetary vorticity and the vertical velocity.

The velocities $\vec{v}_g$ and $\vec{v}_g + A\vec{k}$ are solutions to the same equation if $(2\vec{\Omega}\cdot\vec{\nabla})(\rho\vec{v}_g) = (2\vec{\Omega}\cdot\vec{\nabla})(\rho\vec{v}_g + \rho A\vec{k})$. This requires the derivative of A along the rotation axis to be zero. Thus the indeterminacy A does not contribute to (8).

The right hand side of (8) will be refered to as the baroclinic term $\vec{B}$. Using that $\vec{\nabla}p_h = \rho_h\vec{g} = (\rho - \epsilon_\rho\rho_1)\vec{g}$, the dominant contribution to the baroclinic term is:

$$\vec{B} \equiv \vec{\nabla}\rho\wedge\vec{g} = \frac{\vec{\nabla}\rho\wedge\vec{\nabla}p_h}{\rho - \epsilon_\rho\rho_1} = \frac{1+\epsilon_\rho\frac{\rho_1}{\rho}}{\rho}\vec{\nabla}\rho\wedge\vec{\nabla}p_h + O(\epsilon^2) = -\rho\vec{\nabla}\left(\frac{1}{\rho}\right)\wedge\vec{\nabla}p_h + O(\epsilon^2)$$

Since IR measurements provide temperature information as a function of pressure, it is desirable to express $\vec{B}$ in terms of T and p. For an ideal gas in equilibrium this yields: $\vec{B} = -\rho\frac{R}{M_r}\vec{\nabla}(T/p)\wedge\vec{\nabla}p_h + O(\epsilon^2)$. Our IR measurements are retrieving the temperatures along constant pressure levels, thus p is considered a constant in the previous expression to first order of approximation in ϵ and we write $\vec{B}$ as:

$$\vec{B} = \rho\frac{R}{M_r}\frac{\vec{\nabla}p_h\wedge\vec{\nabla}T}{p_h + \epsilon p_1} + O(\epsilon^2) = \epsilon_T\rho\frac{R}{M_r}\frac{\vec{\nabla}p_h\wedge\vec{\nabla}T_1}{p_h} + O(\epsilon^2).$$

Where $T(x,y,z) = T_h(z) + \epsilon_T T_1(x,y,z) + O(\epsilon^2)$ has been used. Finally, since IR observations are returned on pressure coordinates, one can define pressure coordinates to order ϵ^1 to rewrite the vertical derivative terms as:

$$\frac{1}{\rho}\vec{\nabla}\rho\epsilon v_i \equiv \epsilon\left(\frac{\partial v_i}{\partial x}, \frac{\partial v_i}{\partial y}, \frac{\partial\omega_i}{\partial p_h}\right) + O(\epsilon^2) \equiv \epsilon\vec{\nabla}_p v_i$$

where $\epsilon\omega_i \equiv -g\rho\epsilon v_i = -g\rho_h\epsilon v_i + O(\epsilon^2)$ with v_i being the components of the velocity vector. Using this relation on the left hand side of (8), one can express it in pressure coordinates as:

$$\epsilon(2\vec{\Omega}\cdot\vec{\nabla}_p)\vec{v} = -\frac{\vec{B}}{\rho} = -\epsilon_T\frac{R}{M_r}\left(\frac{\partial ln p_h}{\partial z}\right)\left(\vec{e}_r\wedge\vec{\nabla}T_1\right) + O(\epsilon^2) \tag{9}$$

Direct comparison of these expressions with the familiar expressions (4) show that they coincide at the poles or whenever the meridional changes of velocity are small. This is a gauge for the error introduced in the standard approximation by dropping one component of the Coriolis force. The neglected terms are unimportant in Jupiter at the latitudes where the zonal jets reach their local maximum and minimum velocities. This condition occurs rarely (*Limaye,* 1986).

4.2 Thermal winds with the geopotential formulation

A different approach for getting the vertical changes of the wind is possible with the geopotential formulation. This approach violates (7) since it requires using the hydrostatic approximation in order to permute the vertical and horizontal derivatives of the geopotential. The hydrostatic approximation is inconsistent with (7) but because of its widespread use, it is worth looking at the resulting predictions. (*White & Bromley,* 1995) stated that the errors involved in using the hydrostatic approximation with a full parameterization of the Coriolis force are nevertheless smaller than the error involved in taking the primitive equations.

When the hydrostatic approximation is used, the geostrophic velocity (6) becomes $\vec{v}_g = \frac{1}{2\Omega\rho}\left(-\sin\lambda\frac{\partial\pi_1}{\partial y}, \sin\lambda\frac{\partial\pi_1}{\partial x}, -\cos\lambda\frac{\partial\pi_1}{\partial x}\right)$ which, in terms of the geopotential, reads: $\vec{v}_g = \frac{1}{2\Omega}\left(-\sin\lambda\frac{\partial\Phi}{\partial y}, \sin\lambda\frac{\partial\Phi}{\partial x}, -\cos\lambda\frac{\partial\Phi}{\partial x}\right)$. It is readily seen that this velocity is not a solution to the full geostrophic condition unless condition (7) is introduced through the substitution $\cot\lambda\frac{\partial\pi_1}{\partial y} = \frac{\partial\pi_1}{z} + \frac{\epsilon_\rho}{\epsilon}\rho_1 g$. This substitution is needed only in the zonal component, the meridional and vertical terms remain unaffected. It may be worth noting that the zonal velocity in the standard geostrophic solution also fails to solve the geostrophic equation with a full Coriolis force. The standard result becomes a solution to the full problem when the same substitution is introduced.

Following the same steps as in section 3 for this velocity, one obtains the thermal wind relations:

that can balance the gravity acceleration is the vertical pressure gradient. The Coriolis acceleration is the second most important contribution in the momentum equation but its value is much smaller. The nonhydrostatic correction is given by the ratio of the Coriolis acceleration to gravity, that is, the planetary Froude number $\epsilon \equiv 2U\Omega/g$, which is of the order of $\epsilon \sim 10^{-3}$ for Jupiter. The vertical pressure profile should thus remain close to a hydrostatic profile and geostrophic motion introduces a correction of the order of the Froude number. Table I also shows that one can expect $Ro < 10^{-1}$ and thus $\epsilon \sim 10^{-3} > \epsilon Ro \gtrsim \epsilon^2$ which is consistent with the perturbative series used so far.

The present criterion based on the Froude number does not require shallowness and depends only on the magnitude of the typical velocity U, the acceleration g, and the rotation frequency Ω.

5.2 Ageostrophic contributions

The geostrophic equations are a linear approximation, both in the traditional and in the 3-d model. Their accuracy is limited by the amplitude of the nonlinear terms which, themselves, depend on the solution. Perturbative arguments can be used to estimate the magnitude of the higher order terms in the momentum equation.

Expression (6) for the geostrophic velocity can be used to estimate the advection term. Let us define $\vec{v} \equiv \epsilon(\vec{v}_g + Ro\vec{v}_a)$ (where $\vec{v}_a$ is the ageostrophic contribution to the total velocity), we can write the nonlinear advection term as:

$$(\vec{v} \cdot \vec{\nabla})\vec{v} = \epsilon^2[(\vec{v}_g \cdot \vec{\nabla})\vec{v}_g + Ro(\vec{v}_g \cdot \vec{\nabla})\vec{v}_a + Ro(\vec{v}_a \cdot \vec{\nabla})\vec{v}_g] + O(\epsilon^2 Ro^2, \epsilon^3)$$

From our scale analysis, Ro is $\leq 10^{-1}$. Therefore, the main contribution to advection is given by the geostrophic velocity and is of order ϵ^2. Using (6) with the measurements in hand, one can now understand the existing evidence of why linear models have been so successful at the scale of the measurement resolution: the dominant horizontal temperature gradients are latitudinal, thus so are the gradients of the pressure anomalies.

data with emission angles greater than 60°, and thus the combined maps are cut off near for latitudes greater than $\sim 60°$.

The composite global temperature maps were formed from data taken as much as 5 days apart. Previous studies of the rotation rates of the longitudinal feature seen in the temperature structure (*Deming et al.,* 1989; *Deming et al.,* 1997; *Magalhães et al.,* 1989; *Magalhães et al.,* 1990; *Orton,* 1994) report rotation rates of $\sim$10 m s^{-1}. Such a rotation rate produces a longitudinal smearing of 4300 km ($\sim 3.5°$) over our maximum time difference of five days. This is comparable to our diffraction-limited spatial resolution of $\sim$ 4700 km. Examining the overlapping longitudinal regions of our data show that actual shifts of discrete, identifiable, features was typically much less than the smearing size of 3.5°. While it is still possible that evolution of the temperature field could have occurred within the period spanned by the data, we did not observe any such evolution above our noise level.

7 Results

7.1 Thermal winds

Figures 2a-2d and 3a-3d show the thermal winds along the rotation axis (10). These are the consistent approach to geostrophic thermal winds with a full Coriolis force.

All of the figures use the same scaling to facilitate the comparison of relative amplitudes. Banded structures are apparent in the zonal winds at most latitudes. Meridional winds appear rather constant. Longitudinal structures are apparent in both. Such longitudinal structures are not visible in zonal mean data.

7.2 Thermal winds with the hydrostatic approximation

In order to make a comparison with results based on the primitive equations, figures 4a-4d, 5a-5d, 6a-6d, and 7a-7d show the thermal winds (12) along the vertical when the hydrostatic approximation is used. Figures 4a-4d, compare the familiar result based on the primitive equations, (valid when the meridional velocity gradients are negligible) in

from the full 3-d equations for atmospheric flow have been applied for the first time on diagnostics of Jupiter's upper troposphere.

The development of a 3-d geostrophic formulation for atmospheric diagnostics has resulted in new sets of thermal wind relations (10) and (12). The connections between the traditional and the global scale formulations of geostrophy have been discussed.

The hydrostatic approximation has been shown to be incompatible with a full Coriolis representation of geostrophy in a stratified atmosphere. In the alternative to the hydrostatic approximation, a cylindrical symmetry is introduced by relation (7). Another result is that vertical wind shears may be several times smaller than previously thought, depending on the latitude. 3-d geostrophy has also provided information on the vertical derivatives of the three components of the geostrophic wind. This may be useful to infer vertical transport.

Both, geostrophic balance and the hydrostatic approximation have been standard unquestioned assumptions, but criterion (7) makes incompatible their simultaneous use. There are many other aspects of the dynamics that are not being considered, like nonlinear effects, the fact that the dynamics is not isentropic, the effects of large scale eddy viscosity, or the interaction of the different volatiles. If the pressure field is predominantly defined either by geostrophy or by the hydrostatic profile can be answered only from additional observational evidence. This has been provided only at one location (*Atkinson et al.,* 1998), but one needs to compare large extensions to validate the predictions of geostrophy based on (7) and the hydrostatic approximation.

On the observational side, the thermal wind relations have been used to infer low-noise regularly gridded maps of possible vertical transport at four different pressure levels in the upper Jovian troposphere using ground-based infrared observations. The maps put forward diverse predictions whose validity requires observational confirmation to help to understand the dynamical state of Jupiter at the depth of our observations.

All maps imply a large amount of zonal organization. They also show two relatively

different locations of the updrafts and downdrafts.

The ultimate arbiter of these hypotheses, of course, would be reliable measurements of vertical winds in different regions of Jupiter, and of the pressure and density fields but these are unlikely to be available for some time. The absence of visible tracers at these levels above the clouds make in situ measurements the only candidates to solve these puzzles.

Acknowledgements:

The authors wish to acknowledge the help and support of the staff of the NASA Infrared Telescope Facility for their support of the observations reported here, as well as Dr. Michael Ressler who set up MIRLIN initially in the run, and to Kartik Parija who assisted BMF and GSO in making the observations. MTJ and BMF acknowledge support from the NASA / National Research Council Senior and Postdoctoral Associateships Program. GSO acknowledges support for this work from the Galileo mission and from research grants to the Jet Propulsion Laboratory, California Institute of Technology, from the NASA Planetary Astronomy and Planetary Atmospheres disciplines. The research described in this paper was carried out at the Jet Propulsion Laboratory, California Institute of Technology, under a contract with the National Aeronautics and Space Administration.

References

Atkinson, D.H., J.B. Pollack, A. Seiff, 1998: The Galileo Probe Doppler Wind Experiment: Measurements of the deep zonal winds on Jupiter. *J. Geophys. Res.*, **103**, 22911-22928.

Banfield, D, P.J. Gierasch, S.W. Squyres, P.D. Nicholson, B.J. Conrath, K. Matthews 1996. 2 μm Spectrophotmetry of Jovian Stratospheric Aerosols–Scattering Opacities, Vertical Distributions, and Wind Speeds. *Icarus*, **121**, 380- 410.

Brummel, N.H., N. E. Hurlburt, J. Toomre. 1996: Turbulent compressible convection

Fisher, B. M., G. S. Orton, M. Ressler, S. Hinkley. 1997. Jovian tropospheric horizontal and vertical temperature structure during the Galileo G1 orbit. *Bull Amer. Astron. Soc.*, **29**, 1007.

Gierasch, P.J., B. J. Conrath, J. A. Magalhães. 1986. Zonal mean properties of Jupiter's upper troposphere from Voyager infrared observations. *Icarus 67*, 456-483, 1986.

Gierasch, P.J., B. J. Conrath, 1993. Dynamics of the atmospheres of the outer planets - post-Voyager measurement objectives. *J. Geo. Res. 98*, 5459-5469.

Gill, A.E. 1982. *Atmosphere-Ocean Dynamics*, Academic Press Inc.

Glatzmaier, G.A., P. H. Roberts. 1997. Simulating the geodynamo, *Contemporary Physics* **38**, 269-288.

Holton, J.R. 1992: *An Introduction to Dynamic Meteorology*, 3rd ed. Academic Press Inc, San Diego.

Houghton, J.T. 1986: *The Physics of Atmospheres*, 2nd ed. Cambridge University Press.

Hubbard, W.B. 1998. Gravitational Signature of Jupiter's Deep Zonal Flows. *Bull. Amer. Astron. Soc.* **30**.

Ingersoll, A.P., D. Pollard, 1982. Motion in the interiors and atmospheres of Jupiter and Saturn: Scale analysis, anelastic equations, barotropic stability criterion. *Icarus* **52**, 62-80.

Ingersoll, A.P., C.C. Porco, 1978. Solar heating and Internal Heat flow on Jupiter. *Icarus* **35**, 27-43.

Landau, L.D., E.M. Lifshitz 1987. *Fluid Mechanics*, 2nd ed. Pergamon Press, Oxford.

Limaye, S., 1986. Jupiter: New estimates of the mean zonal flow at the cloud level. *Icarus* **65**, 335-352.

Magalhães, J. A., A. L. Weir, P. J. Gierasch, B. J. Conrath, S. S. Leroy. 1989. *Nature* **337**, 444-447.

White, A.A., R.A. Bromley, 1995. Dynamically consistent, quasi-hydrostatic equations for global models with a complete representation of the Coriolis force. *Q. J. R. Meteorol. Soc.* **121**, 399-418.

Williams, G.P., Robinson, J.B., 1973. Dynamics of a convectively unstable atmosphere: Jupiter ? *J. Atmos. Sci.* **30**, 684-717.

Williams, G.P. 1996. Jovian Dynamics. Part I: Vortex stability, structure and genesis. *J. Atmos. Sci.* **53**, 2685-2734.

Yano, J-I., 1994. A critical review on the dynamics of Jovian atmospheres. *Chaos* **4**, 287-297.

Zhang, K., G. Schubert. 1996. Penetrative convection and zonal flow on Jupiter. *Science* **273**, 941-943.

Figure Captions

Figure 1. Composite global temperature maps as a function of planetocentric latitude and west System III longitude. Note the the bright feature near 25° W, 25° N, is the Jovian moon Io which was transiting during the observation.

Figure 2. The zonal component of the geostrophic wind shear, $\partial u_g/\partial Z^*$, for each pressure level.

Figure 3. The meridional component of the geostrophic wind shear, $\partial v_g/\partial Z^*$, for each pressure level.

Figure 4. Mean zonal values of the zonal component of the geostrophic wind shear, $< \partial u_g/\partial z^* >$, for the upper and lower pressure levels, compared to the cloud derived winds (solid line) from Limaye 1986. Results using the classical hydrostatic approximation are shown as filled circles. Results using equation (7) are shown as open squares. The upper two panels are scaled to show the full range. The lower panels are scaled to show the details of the small amplitude structure. Panel (a) corresponds to the 100 mbar pressure level, (b) to 400 mbar , (c) to 100 mbar, and (d) to 400 mbar.

Figure 5. The zonal component of the geostrophic wind shear, $\partial u_g/\partial z^*$, for each pressure level.

Figure 6. The meridional component of the geostrophic wind shear, $\partial v_g/\partial z^*$, for each pressure level.

Figure 7. The vertical component of the geostrophic wind shear, $\partial w_g/\partial z^*$, for each pressure level.

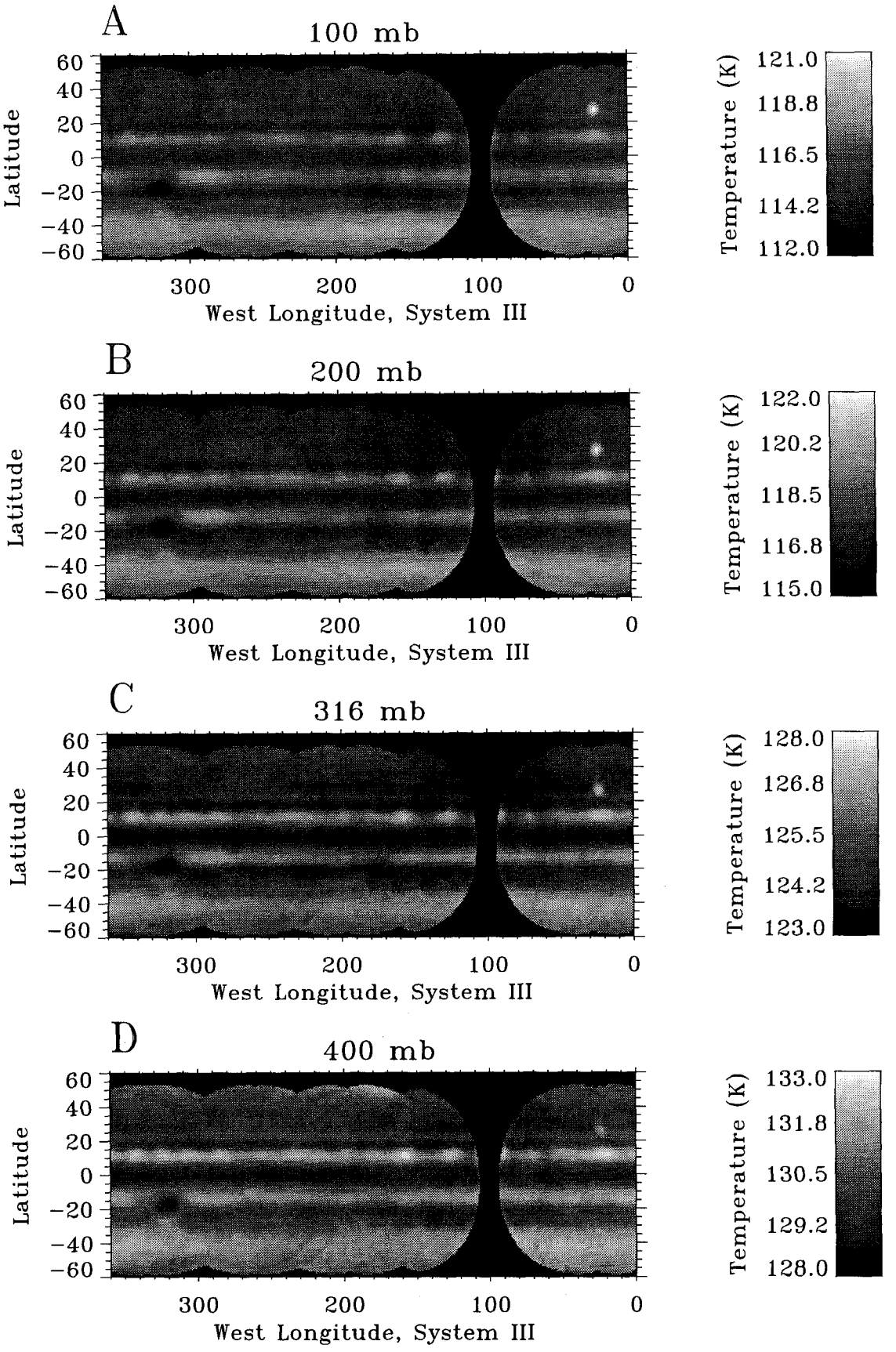
A
100 mb
Latitude
60
40
20
0
-20
-40
-60
300
200
100
0
West Longitude, System III
Temperature (K)
121.0
118.8
116.5
114.2
112.0
B
200 mb
Latitude
60
40
20
0
-20
-40
-60
300
200
100
0
West Longitude, System III
Temperature (K)
122.0
120.2
118.5
116.8
115.0
C
316 mb
Latitude
60
40
20
0
-20
-40
-60
300
200
100
0
West Longitude, System III
Temperature (K)
128.0
126.8
125.5
124.2
123.0
D
400 mb
Latitude
60
40
20
0
-20
-40
-60
300
200
100
0
West Longitude, System III
Temperature (K)
133.0
131.8
130.5
129.2
128.0

Figures 1 a-d

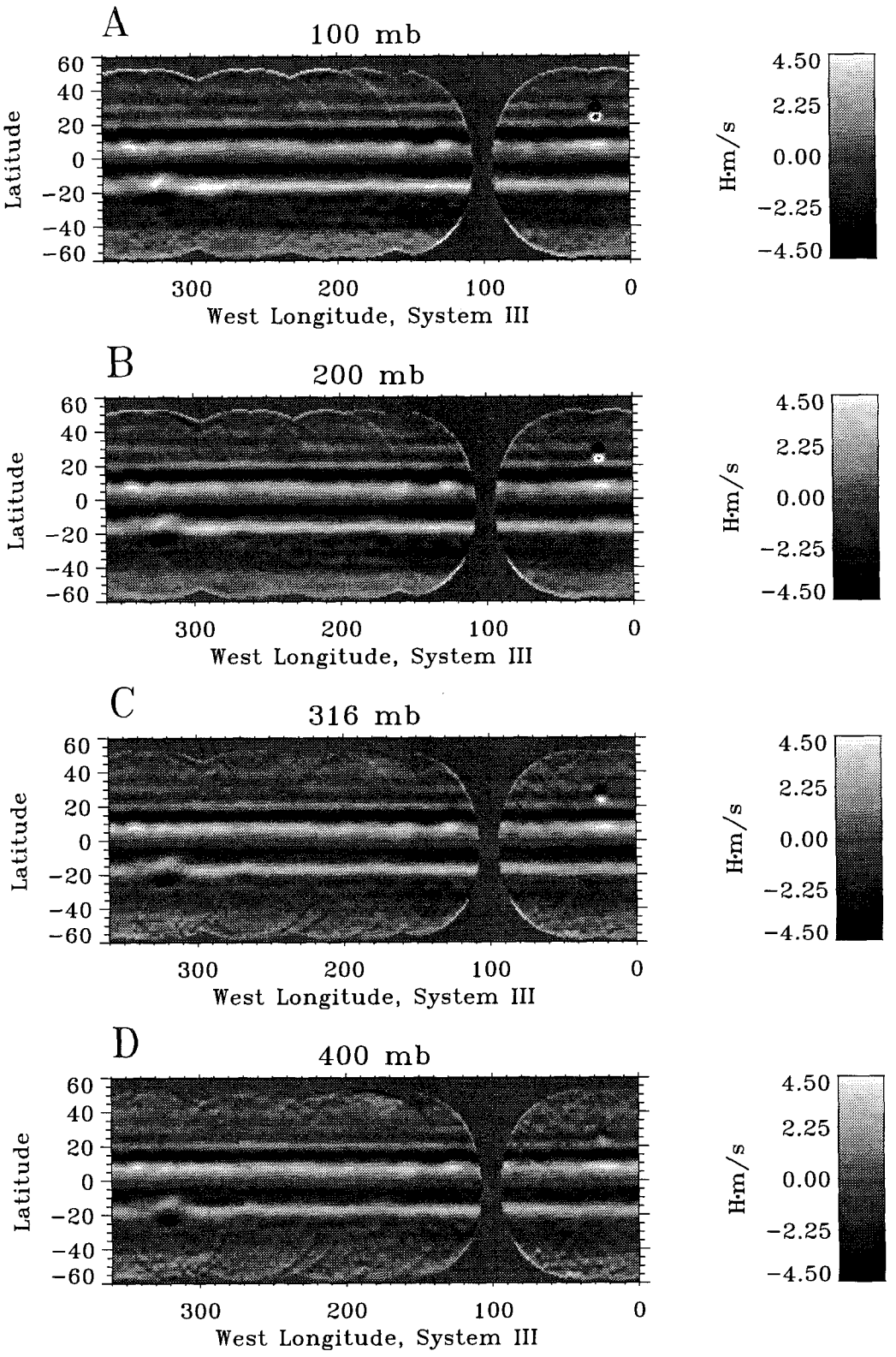
A
100 mb
B
200 mb
C
316 mb
D
400 mb
Latitude
60
40
20
0
-20
-40
-60
300
200
100
0
West Longitude, System III
H·m/s
4.50
2.25
0.00
-2.25
-4.50

Figures 2a-d

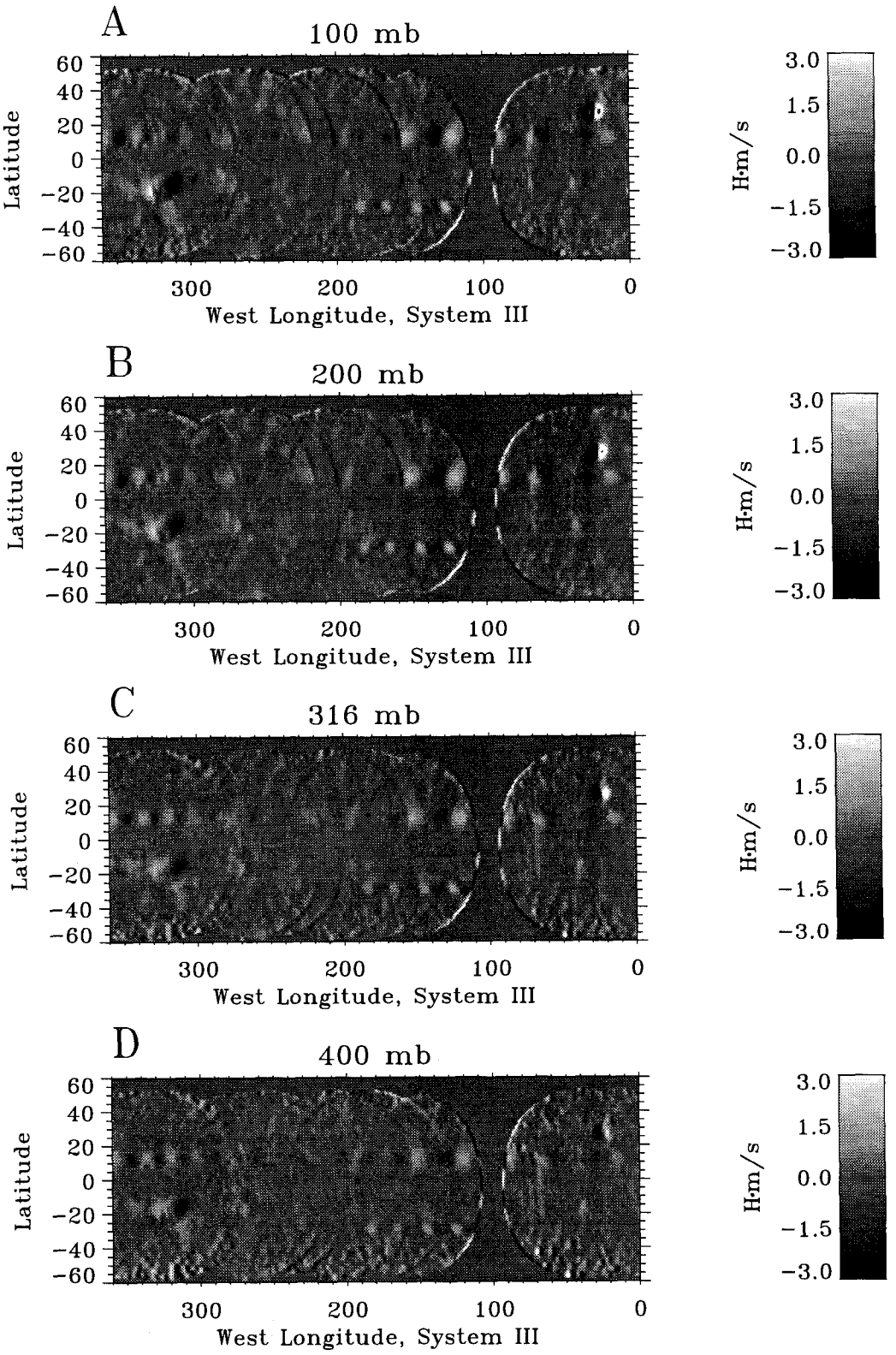
A
100 mb
B
200 mb
C
316 mb
D
400 mb
Latitude
60
40
20
0
−20
−40
−60
300
200
100
0
West Longitude, System III
H·m/s
3.0
1.5
0.0
−1.5
−3.0

Figures 3a-d

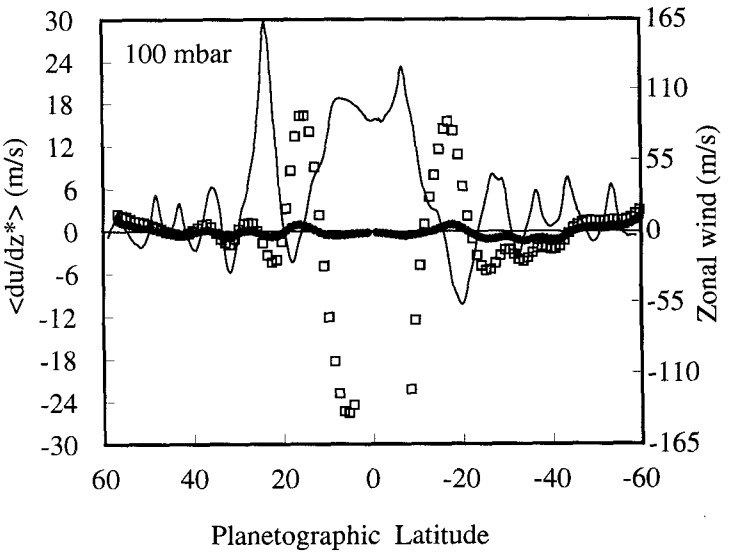

Figure 4a

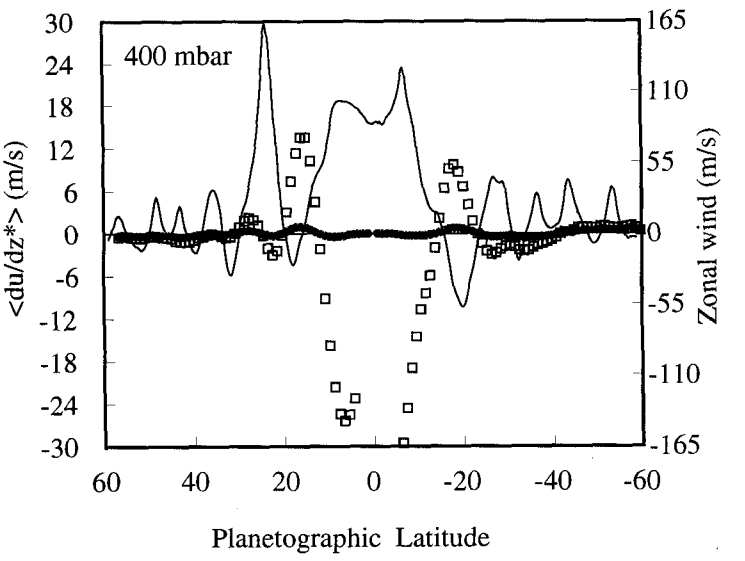

Figure 4b

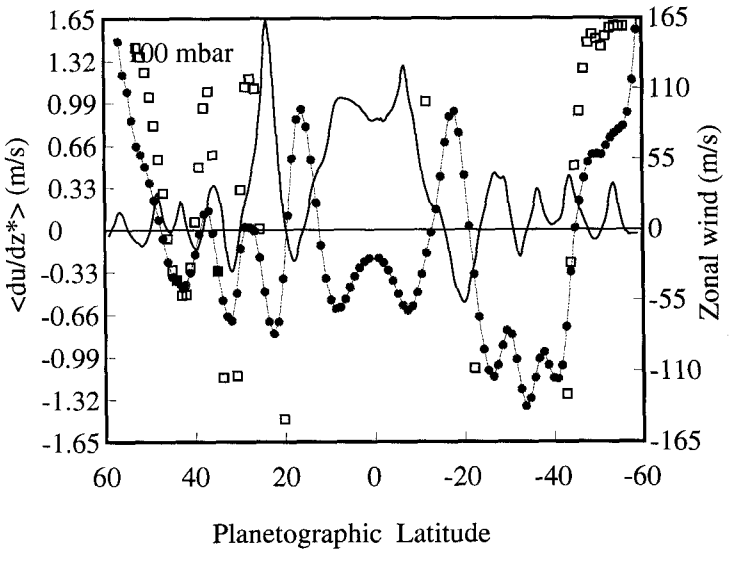

Figure 4c

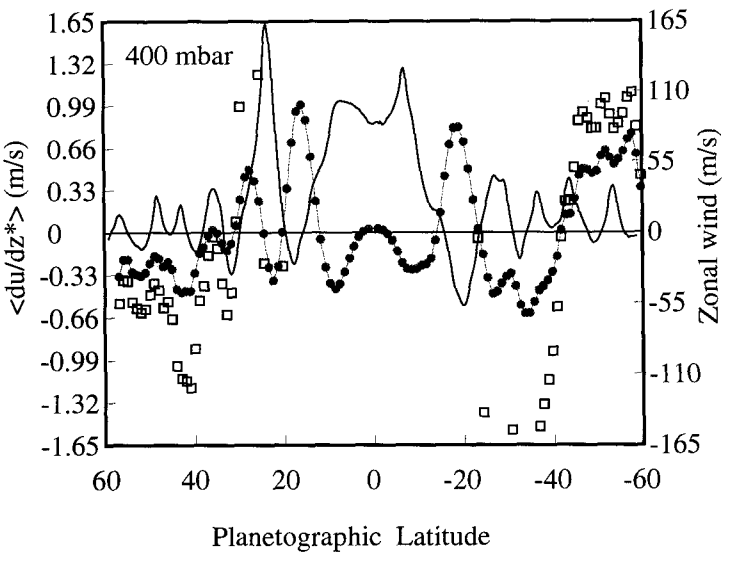

Figure 4d

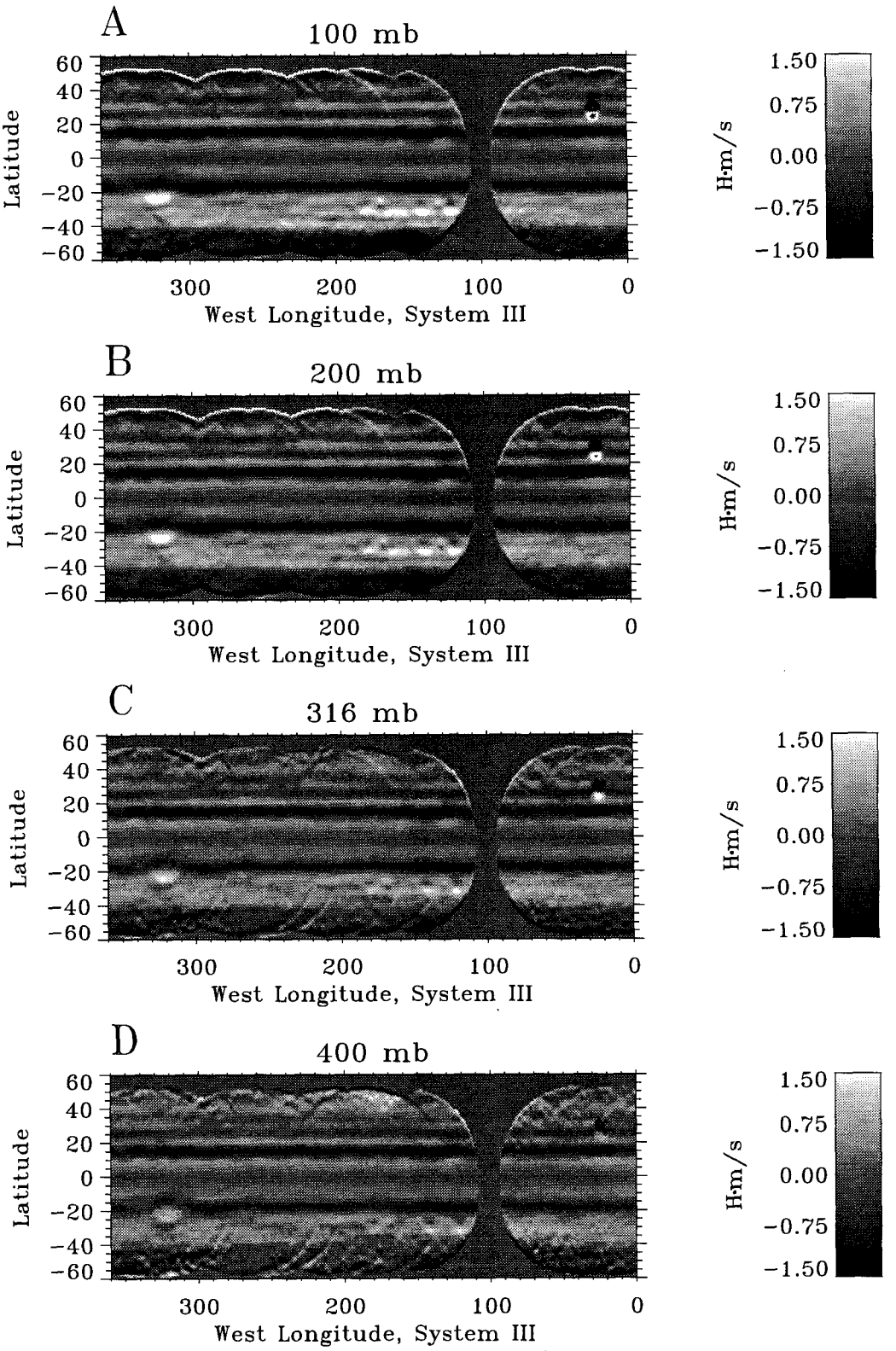
A
100 mb
B
200 mb
C
316 mb
D
400 mb
Latitude
60
40
20
0
-20
-40
-60
300
200
100
0
West Longitude, System III
H·m/s
1.50
0.75
0.00
-0.75
-1.50

Figures 5a-d

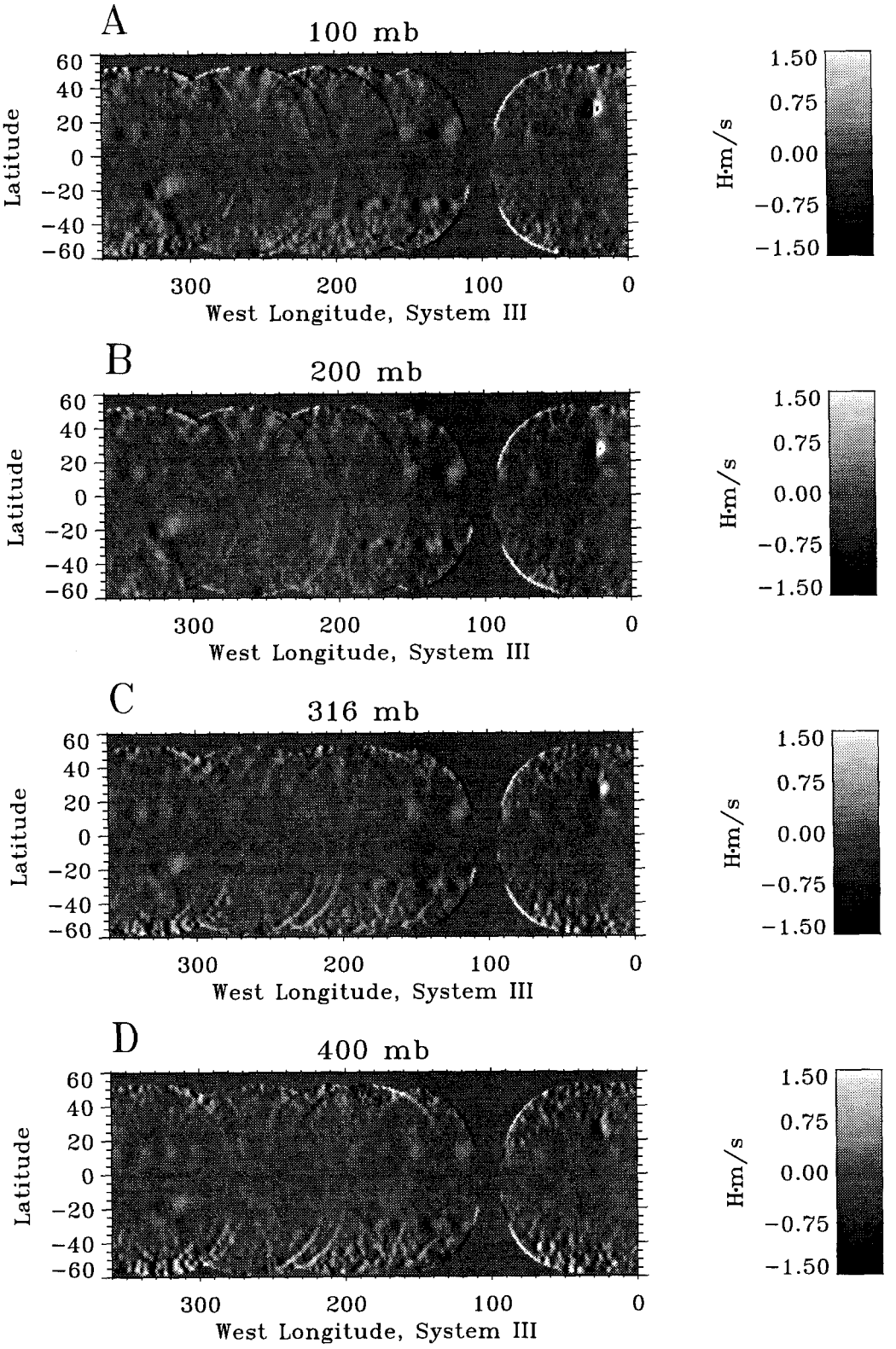
A
100 mb
B
200 mb
C
316 mb
D
400 mb
Latitude
60
40
20
0
−20
−40
−60
300
200
100
0
West Longitude, System III
H·m/s
1.50
0.75
0.00
−0.75
−1.50

Figures 6a-d

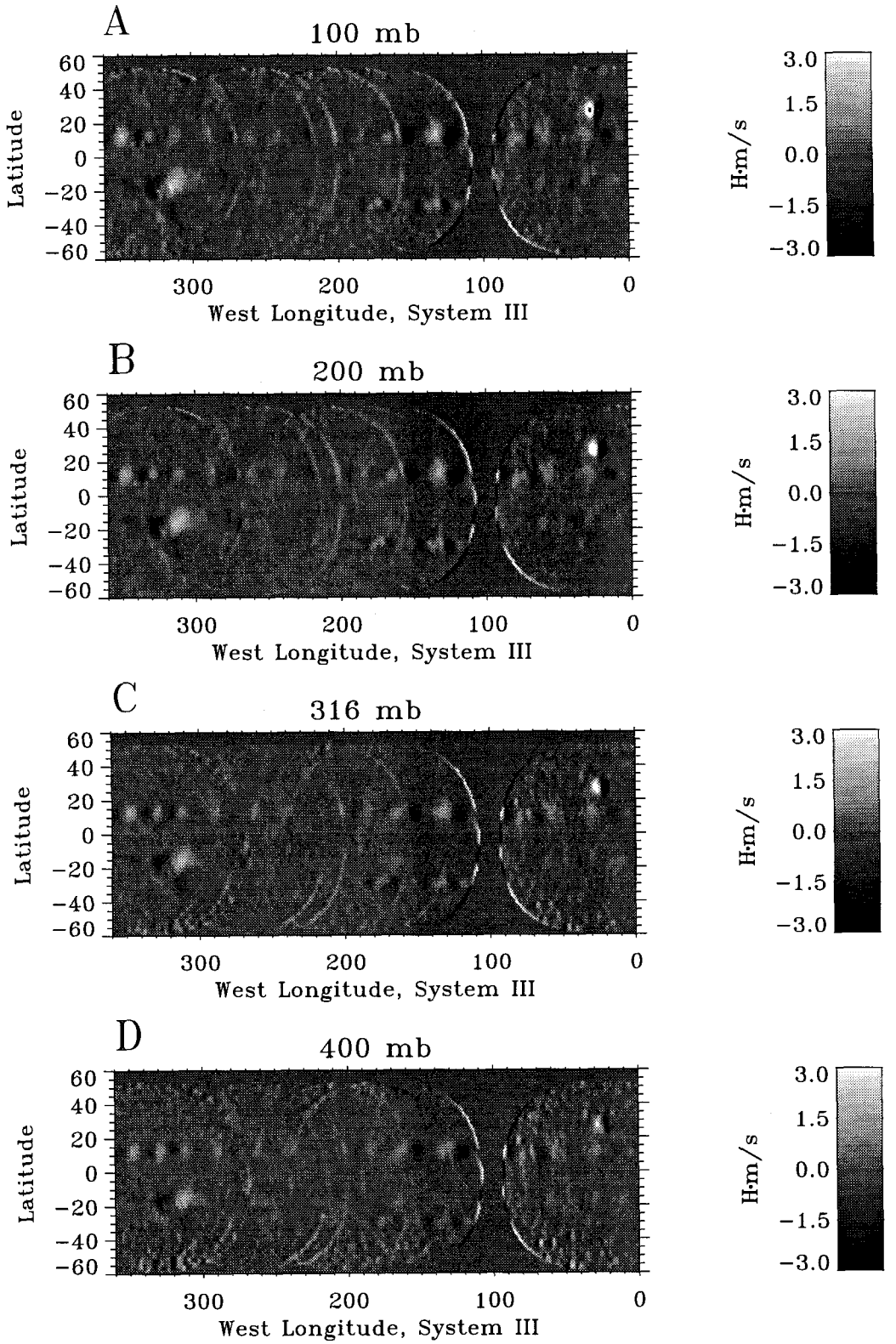
A
100 mb
B
200 mb
C
316 mb
D
400 mb
Latitude
60
40
20
0
−20
−40
−60
300
200
100
0
West Longitude, System III
H·m/s
3.0
1.5
0.0
−1.5
−3.0

Figures 7a-d